

FIG. 7. Histograms of the distribution of interaction strengths for the experimental data shown in the main text. The histograms are obtained by averaging over 50 distributions of interaction strengths, with a bin size of $0.1 \text{ median}_j \max_i |J_{i,j}^{\perp}|$.

APPENDIX D: INFLUENCE OF THE GAUSSIAN TRAP GEOMETRY ON THE RELAXATION DYNAMICS

The functional form of the relaxation dynamics in a strongly disordered spin system has been demonstrated to be independent of both the Rydberg blockade radius and the anisotropy of the Heisenberg XXZ Hamiltonian. However, the timescale of these dynamics is contingent upon the density and coupling constant. Consequently, there arises the necessity to rescale time by the median interaction strength $\text{median}_i \max_j J_{ij}$.

In the context of a Gaussian trap geometry, we conduct an averaging procedure over varying local densities ρ . Assuming local density approximation, we average over different local relaxation dynamics, each characterized by a stretched exponential function, sharing a common stretching exponent β , while exhibiting distinct timescales $\tau(\rho)$. The collective summation of these relaxation curves again manifests as a stretched exponential decay. However, the details of the stretching exponent β depend on the shape of the Gaussian cloud (cf. Fig. 8).

Furthermore, finite-size effects come into play, with one-dimensional physics becoming relevant in an elongated cigar-shaped geometry and two-dimensional physics in a flat pancake geometry. Consequently, the measured stretched exponential does not align with the expected value of $\beta = d/\alpha$ (where d represents the dimension and α signifies the range of interactions) as anticipated from semiclassical simulations [28]. Instead, the observed value interpolates between various dimensions and exhibits slight variations in different experimental realizations when the trap geometry is altered.

Nevertheless, through a comparative analysis of experiments conducted in similar geometries, it remains feasible to investigate whether the dynamics are contingent upon the size of the blockade radius [21] or the anisotropy parameter Δ of the Heisenberg XXZ Hamiltonian (as explored in this study).

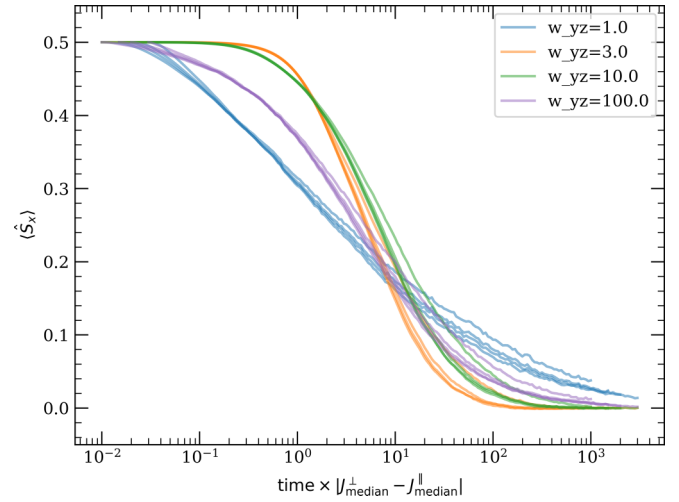


FIG. 8. MACE simulations of the relaxation of the magnetization for four different geometries of the Gaussian cloud where the aspect ratio of the waist w_x in x direction with respect to the waist w_{yz} in y and z direction is tuned. The product $w_x \times w_{yz}^2$ is fixed for all four geometries. For each geometry, we simulate the time evolution for different anisotropies $J_{\perp}^{\parallel} \in \{-2, -0.5, 0, 0.5, 2\}$.

APPENDIX E: RELAXATION UNDER INITIAL STATES WITH DIFFERENT MAGNETIZATION

In order to test if the universal relaxation behavior, originating from a pair picture approximation is even consistent for the relaxation of more general states than the fully

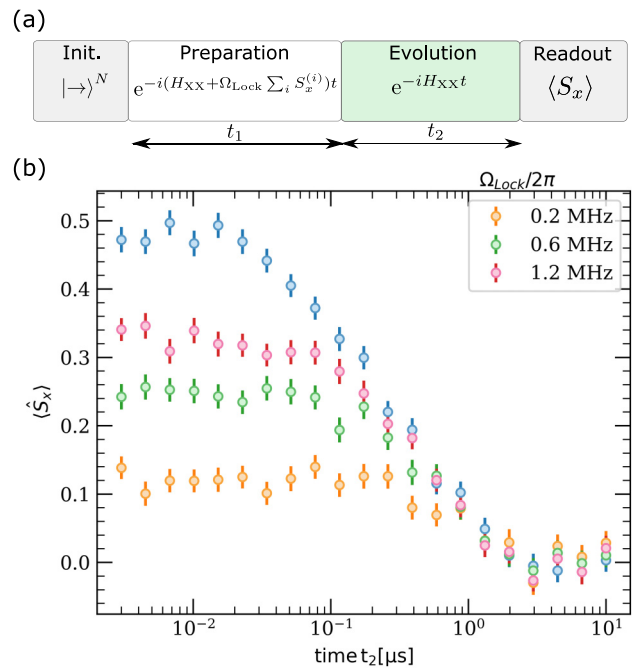


FIG. 9. Relaxation dynamics of initial states with different magnetization. (a) Experimental sequence consisting of an evolution under a spin locking field (preparation), followed by a measurement of the magnetization for the resulting relaxation dynamics for t_2 (evolution). (b) Magnetization dynamics after different $\Omega_{\text{Lock}}/2\pi$ applied in phase one.